Microchim Acta (2017) 184:4647–4654
DOI 10.1007/s00604-017-2506-7

ORIGINAL PAPER

Molybdenum disulfide quantum dot based highly sensitive impedimetric immunoassay for prostate specific antigen

Manil Kukkar[1,2] · **Suman Singh**[1,2] · **Nishant Kumar**[1] · **Satish K. Tuteja**[3] · **Ki-Hyun Kim**[4] · **Akash Deep**[1,2]

Received: 5 June 2017 / Accepted: 7 September 2017 / Published online: 16 September 2017

Abstract This work reports on the synthesis of molybdenum disulfide quantum dots (MoS_2-QDs) from pre-exfoliated MoS_2 nanosheets. After a thorough characterization, the MoS_2-QDs were assembled onto screen-printed carbon electrodes, followed by the physical adsorption of antibodies against the prostate-specific antigen (PSA) to form a bioelectrode. Because of the hydrophobic nature of the QDs, they are favorable for the hydrophobic interaction with the antibodies. Based on cyclic voltammetry (CV) and electrochemical impedance spectroscopy (EIS) techniques, the bioelectrode was employed for the detection of PSA using hexacyanoferrate as the redox probe. The electrode yielded an optimum CV response of PSA in the range of 0.1 pg·mL^{-1} to 10 ng·mL^{-1} (scan rate: 0.05 mVs^{-1}). The performance improved significantly when EIS was applied (response range: 0.01 pg·mL^{-1} to 200 ng·mL^{-1}; limit of detection: 0.01 pg·mL^{-1}). The feasibility of the immunoassay was demonstrated by successfully analyzing PSA in serum samples based on the standard addition method. A near 100% recovery of PSA from the serum samples supports the possible practical viability of the procedure. The immunoassay highlights a number of advantageous features such as convenient attachment of antibodies over the electrode surface and broad range of PSA detection with the successful demonstration with real serum samples.

Keywords Molybdenum disulfide · Quantum dots · Impedance spectroscopy · Voltammetry · Immunoassay · Prostate-specific antigen · Nyquist plot · Nanosheets

Manil Kukkar and Suman Singh contributed equally to this work.

Electronic supplementary material The online version of this article (https://doi.org/10.1007/s00604-017-2506-7) contains supplementary material, which is available to authorized users.

✉ Ki-Hyun Kim
kkim61@hanyang.ac.kr

✉ Akash Deep
dr.akashdeep@csio.res.in

[1] CSIR-Central Scientific Instrument Organisation (CSIR-CSIO), Chandigarh 160030, India

[2] Academy of Scientific and Innovative Research (AcSIR-CSIO), Chandigarh 160030, India

[3] BioNano Laboratory, School of Engineering, University of Guelph, Guelph, ON N1G 2W1, Canada

[4] Department of Civil and Environmental Engineering, Hanyang University, 222 Wangsimni-Ro, Seoul 04763, South Korea

Introduction

Transition layered materials (TMD: e.g., MoS_2, WS_2, VS, WSe_2, $MoSe_2$, and TiS_2) have achieved paramount significance in many diverse fields of research. A member of this family, molybdenum disulfide (MoS_2), comprised of three atom layers (S–Mo–S) stacked together through van der Waals interactions, has gained immense popularity due to its distinctively advantageous properties, e.g., its electronic band transformation from an indirect gap to a direct gap, robust mechanical strength, and superior electrical performance [1, 2]. These features have been observed in photovoltaic, nanoelectronics, energy storage, solar cells, catalysis and biosensing applications [3–5]. The application of MoS_2 nanomaterials in biosensing was first reported in 2013, and significant developments in this research area have been recorded since then [6, 7]. Even when compared to another very promising 2D material 'graphene', MoS_2 nanostructures have been

advocated to be more beneficial particularly in electronic/electrochemical applications. With the existence of a direct energy band gap, MoS_2-based devices can be switched between electrically conducting and non-conducting states. In contrast, as graphene does not possess energy gap, its devices cannot be fully switched off. Thus, a greater control over the electrical behavior of MoS_2 makes it a more potent candidate for electronic and electrochemical applications.

The usefulness of MoS_2 nanostructures and their composites as electroactive surfaces and substrates has been exploited recently in diverse applications. For instance, hybrid composites of MoS_2 and graphene/reduced graphene oxide have been documented for highly sensitive electrochemical determination of pesticides like methyl parathion, ascorbic acid, dopamine, and uric acid as well as for the solid phase extraction of heavy metals (such as Ni(II) and Pb(II)) [8–10]. In combination with copper sulfide and carbon nanotubes, MoS_2 composites have been used to modify glassy carbon electrodes for enzyme-free amperometric sensing of glucose and hydrogen peroxide [11, 12]. Similarly, glassy carbon electrode modified with layered molybdenum selenide, graphene, and gold nanoparticles was documented for differential pulse voltammetry based assay of carcinoembryonic antigen [13]. Likewise, in a recent study, a glassy carbon electrode was modified with MoS_2 nanosheets and poly(3,4-ethylenedioxythiophene) for simultaneous electrochemical detection of ascorbic acid, dopamine, and uric acid [14]. The application of MoS_2 modified glassy carbon electrode was also reported for the detection of bisphenol [15]. In that particular study, a nanocomposite of MoS_2, intercalated into self-doped polyaniline, was used. MoS_2 nanoflowers, in combination with graphene and carbon nanotube, have also been reported for the sensing of dopamine [16]. The peroxidase-like activity of MoS_2 has been reported to be useful for the colorimetric assay for cholesterol [17]. Those previous studies clearly support the fact that the MoS_2 nanostructures should be highly useful for the electrochemical biosensing applications. However, many of those studies appear to suffer in that they were unable to avoid the problem of interferences from commonly associated species.

Although the synthesis of 2D–layered TMD materials (including MoS_2) has been widely reported, relatively little has been reported on the synthesis of Zero Dimensional (0D) MoS_2 quantum dots (QDs) [18–20]. The potentially advantageous properties of MoS_2-QDs (e.g., a very large (hydrophobic) surface area, enhanced catalysis, electronic properties and edge atoms) should be attractive for bioassay applications where MoS_2 nanosheets are generally explored for similar purposes. MoS_2-QDs are the zero dimensional material with entirely special electronic properties (e.g., quantum confinement effect, edge effects, large edge-to-volume ratios, and high in-plane electron transport abilities) relative to other MoS_2 nanostructures. For instance, because of quantum confinement effect, MoS_2-QDs can exhibit an increased band gap than the monolayer 2D sheets. An improvement in electrocatalytic activity of the MoS_2-QDs (relative to their layered counterparts) can be ascribed to a larger number of exposed active sites and high in-plane electron transport. As such, MoS_2-QDs are characterized with enhanced breakage of intra-plane S–Mo–S bonds to produce more edge atoms which also results in a high surface area. Further, due to the subsequent lack of co-ordination of the surface atoms, the density of unsaturated bonds increases in MoS_2-QDs. Thereby, the resulting enhanced surface activity becomes beneficial for both electrocatalytic properties of the electrode and bioconjugation of proteins assisted by hydrophobic interaction.

In the presented work, MoS_2-QDs are synthesized and then exploited for electrochemical detection of prostate-specific antigen (PSA). Prostate cancer is the second leading cause of all cancer-related deaths in men [21]. Elevated PSA is one of the most validated serum markers for the early diagnosis of prostate cancer. A PSA concentration greater than 4 $ng \cdot mL^{-1}$ is interpreted as a sign of a possible tumor in the prostate. Hence, measurement of its concentration in blood samples is one of the most widely used methods to screen for the disease [22]. The conventional techniques for the clinical measurement of PSA, such as chromatography or enzyme-linked immunoassay (ELISA), have a number of limitations such as high cost, lengthy analysis time, and bulky instruments. Thus, these conventional methods are not necessarily suitable for routine screening applications or point-of-care diagnostics. Therefore, the development of rapid diagnostic test that can be applied for the early determination of PSA is considered a highly attractive field of research. In this regard, electrochemical-based diagnostic tools are promising options due to their convenient handling, simplicity, potential for miniaturization, fast response, and relatively low device cost. This work demonstrates the application of MoS_2-QDs for sensitive, convenient, and electrochemical impedance spectroscopy-based immunoassay for PSA.

Material and methods

Materials and equipment

Prostate-specific antigen (PSA) was procured from MP Biomedical, USA (https://www.mpbio.com). Polyclonal anti-PSA antibodies, human serum albumin (HSA), carcinoembryonic antigen, IgG and alpha-fetoprotein (AFP) were purchased from Sigma, India (http://www.sigmaaldrich.com/india.html). The salts for the phosphate buffer, viz., K_2HPO_4 and $KHPO_4$, potassium chloride (KCl), potassium ferrocyanide [$K_4Fe(CN)_6$], and potassium ferricyanide [$K_3Fe(CN)_6$], were purchased from Himedia Pvt. Ltd., India (http://www.himedialabs.com). Screen-printed carbon electrodes (SPCE, surface

area of working electrode = 0.1256 cm^2) were purchased from Zensor, Taiwan (www.zensor.com.tw). De-ionized water from a Millipore water purifier was used for all solution and dilutions.

A probe sonicator (VC 750, Sonics, www.sonics.com) was used for the synthesis of MoS_2-QDs. The instrument employed a 25 mm-diameter probe which was operated with a variable amplitude power supply output at a pulse rate of 8 s (on) or 2 s (off). The size and morphology of the MoS_2-QDs were determined with High Resolution Transmission Electron Microscopy (HR-TEM, FEI Tecnai G2-F20, USA, www.fei.com) and Scanning Electron Microscopy (FE-SEM, 4300S, Hitachi, Japan, www.hitachi-hightech.com). The light absorbance properties were studied with a UV-visible spectrophotometer (U-3900H, Hitachi, Japan, www.hitachi-hightech.com), while the fluorescence measurements were performed on a fluorescence spectrophotometer (Varian Cary Eclipse, Agilent, USA, www.agilent.com). The contact angle and surface energy studies were performed with a Kruss Drop Shape Analysis System (DSA 100, Germany, www.kruss.de) using the sessile-drop technique. The diffraction patterns were recorded with an X-Ray diffractometer (XRD, Rigaku Ultima IV, Japan, www.rigaku.com). Raman spectra were collected with the Raman spectrophotometer (Invia, Renishaw, UK, www.renishaw.com), and topography information was studied with an atomic force microscope (AFM, XE-NSOM, Park Systems, Korea, www.parkafm.com).

The electrochemical measurements were performed on a potentiostat system (CH Instruments: Model-1100, USA, www.chinstruments.com). Impedance spectra were recorded on an impedance analyzer (CH Instruments: Model-660 C, USA, www.chinstruments.com) over a frequency range of 1.0 to 10^5 Hz at a fixed AC voltage of 10 mV in phosphate buffer containing 1.0 mM ferro/ferricyanide $[Fe(CN)_6]^{3-/4-}$ redox couple (hexacyanoferrate II/III). Human serum samples of healthy subjects were obtained from Public Computerized Laboratory, Fatehgarh Sahib, Punjab (India).

Synthesis of MoS_2 quantum dots

The MoS_2-QDs were prepared by probe sonication of electrolytically-synthesized MoS_2 nanosheets. The process of electrolytic synthesis of MoS_2 nanosheets was reported in our previous work [23]. Briefly, the cathodic intercalation of Na^+ ions into the raw molybdenum sheet was conducted using chrono-amperometry at a constant potential of 1.0 V. The Na^+ intercalated MoS_2 sheets were sonicated for 2 h to obtain exfoliated MoS_2 nanosheets. After the formation of MoS_2 nanosheets, the samples were subsequently probe-sonicated for 2 h (at an amplitude of 98%, frequency of 20 kHz, and solution temperature < 20 °C) to obtain the QDs through reduction of atomic size. The selection of suitable temperature and amplitude conditions is a crucial part of the probe sonication process. As the final properties of materials can be altered by an increase in liquid temperature (e.g. due to the churning effect), temperature needs to be controlled. The amplitude, on the other hand, can influence the particle size [24]. The selection of a high amplitude results in a more significant size reduction effect. It should also be mentioned here that the probe was set to operate for 8 s, followed by an intermittent stand-by of 2 s to avoid excessive heating and solvent evaporation. The resulting suspension was left undisturbed to allow the particles to settle out. The supernatant (final product) was recovered by centrifugation at 13,000 rpm (30 min).

Modification of SPCE with MoS_2-QDs and immobilization of anti-PSA

The MoS_2-QDs were decorated on the screen-printed carbon electrode (SPCE) via drop casting. Here, highly delocalized p conjugation in the SPCE surface interacted with outer electrons of S atom in MoS_2 allowing the formation of a stable compact layer. After drying, the electrodes were washed with a copious amount of DI water. Several such electrodes were prepared in a single batch. The immobilization of PSA antibodies on the MoS_2 SPCEs was carried out via physical adsorption of a protein solution (10 μL, 100 $\mu g \cdot mL^{-1}$). The immobilization of the protein over the MoS_2 surface took place via hydrophobic interactions due to the hydrophobic nature of MoS_2-QDs. The fabricated SPCE/MoS_2-QD/PSA_{Ab} electrodes were washed thoroughly with phosphate buffer (10 mM, pH 7.4) to remove loosely-bound antibody fractions. The step by step process of immunoassay development is depicted in Fig. S1 of Supplementary Information.

Results and discussion

Morphology and structural studies of MoS_2-QDs

The morphology of the MoS_2-QDs was assessed by transmission electron microscopic (TEM) imaging. According to the TEM and high resolution TEM (HR-TEM) analysis, the size of the uniformly-dispersed MoS_2-QDs was in the range of 5–7 nm [Fig. 1 (a) & (b)]. The particle size distribution analysis also indicated the average diameter of the QDs to be around 6 nm [Fig. 1 (c)]. In Fig. 1 (d), a typical d-spacing value of 0.27 nm assigned to a (100) lattice plane indicates the formation of hexagonal lattice-structured MoS_2-QDs [25]. As seen in the inset of Fig. 1 (d), the SAED pattern of the MoS_2 QDs indicates the presence of typical diffraction planes [26]. The MoS_2-QDs were also studied by atomic force microscopy (AFM) (Fig. S2). For the AFM imaging, the sample was drop-cast onto a silicon substrate and then dried with nitrogen. The analysis was carried out using contact mode topography. The analysis shows the presence of uniformly-sized

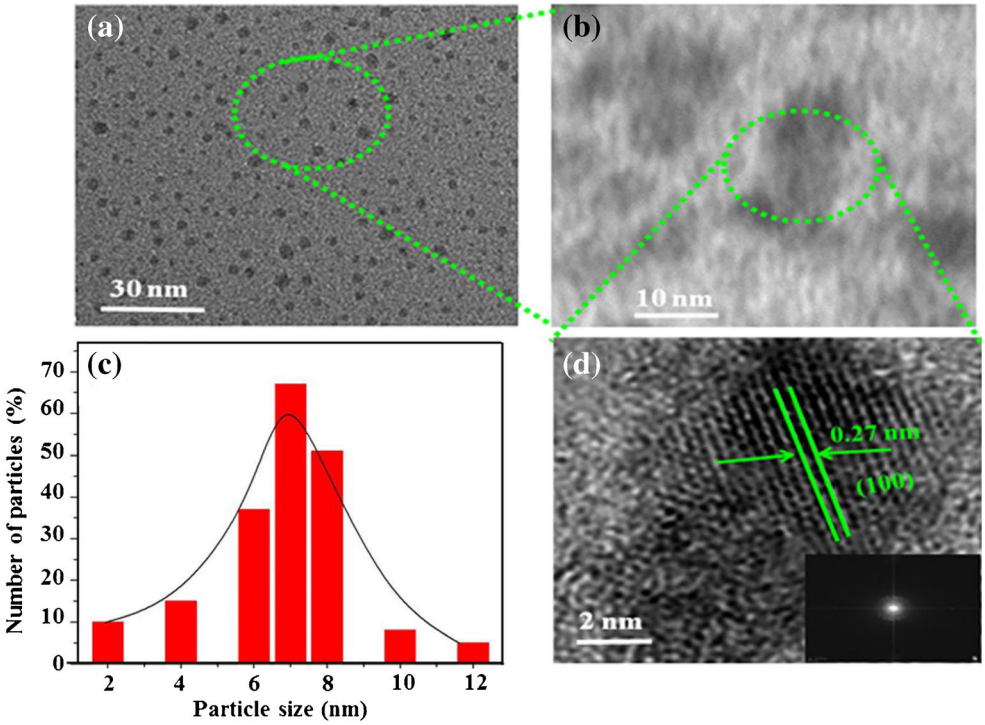

Fig. 1 (**a**) TEM analysis of MoS_2-QDs, (**b**) TEM analysis at a higher resolution, (**c**) particle size distribution of the MoS_2-QDs, and (**d**) HR-TEM and SAED patterns (inset)

particles with spherical morphology. The AFM height/line profile analysis indicates an average size of ~6 nm, while the 3D micrograph depicts the formation of highly uniform MoS_2-QDs.

Contact angle, XRD and Raman spectroscopy studies

Hydrophobic surfaces are known to have a higher affinity for the adsorption of protein than hydrophilic surfaces. To test the potential of MoS_2-QDs for the physical adsorption of proteins, their hydrophobic characteristics were studied using contact angle measurements. Fig. S3 shows the wetting behavior of the bare and MoS_2-QD-modified SPCEs. The contact angle of the MoS_2-QD-modified electrode was found to be 80.07°. This indicates that the MoS_2-QDs improved the hydrophobic nature of the electrode. This degree of hydrophobicity on the electrode surface should facilitate its use as a matrix for antibody adsorption without any further surface treatment [27]. Unlike other nanomaterials (e.g., graphene, CNTs, and CdSe QDs), the MoS_2-QDs electrode does not require any additional surface treatment (e.g., the use of siloxane layers or other treatments to generate functional groups) to avoid the formation of an extra layer between the electrode surface and the charged probe biomolecule. This advantage is expected to yield improved assay sensitivity [20]. Fig. S4(a) shows the Raman spectrum of the MoS_2-QDs. Two main peaks (at 412 and 386 cm^{-1}) corresponding to the Mo–S bonds were assigned to the typical vertical plane (A^{1g}) and in-plane (E^1_{2g}), respectively. In the bulk form of MoS_2, the Raman spectrum typically shows the A^{1g} and E^1_{2g} modes at ~407 and ~383 cm^{-1}, respectively [28]. Both peaks for the MoS_2-QDs sample were red-shifted compared to those of bulk MoS_2. Also, the E^1_{2g}: A^{1g} peak intensity ratio of 0.52 was lower than that of the bulk MoS_2 (0.65). This effect is due to the confinement of the planar vibration mode by the grain distribution and the domain size of QDs [29]. Fig. S4(b) depicts the XRD patterns of the MoS_2-QDs and the bulk MoS_2 sample. The pattern for the bulk sample is comparable with the standard XRD pattern (ICDD ref. no. 04–003-3374). In MoS_2-QDs, the presence of (002) reflection confirms the synthesis of crystalline nanoparticles. The results of EDX and FE-SEM analysis [Figs. S4(c) & S4(d)] of the MoS_2-QDs samples also support the XRD analysis.

Spectral properties of the MoS_2-QDs

In Fig. S5 (a), the UV-visible spectra of the MoS_2 nanosheets and the synthesized QDs are provided. The spectrum of the MoS_2 nanosheets shows the presence of characteristic peaks at 400, 450, 610 and 670 nm. The peaks at 612 and 670 nm correspond to direct excitonic transitions at the Brillouin zone K point in MoS_2 [30] and are typical characteristics of exfoliated MoS_2 in solution [31]. The peaks at 400 and 450 nm correlate with the direct transition from the deep valence band to the conduction band. In the case of MoS_2-QDs, an additional broad shoulder is observed at about 270 nm, which might have arisen from their distinct excitonic features [31, 32]. Fig. S5(b) shows the photoluminescence (PL) spectrum of the MoS_2-QDs, characterized with a broad emission peak at 485 nm representing excitation by light energy at 390 nm. The

PL emission peak of the electrolytically-synthesized MoS_2 nanosheets, as reported in our previous report [33], appeared at a higher wavelength (670 nm). The blue shift of the PL emission wavelength of the MoS_2-QDs can be attributed to the surface charge recombination associated with the quantum confinement effect [34].

Electrochemical characterizations

The electrochemical characterizations of the MoS_2-QD modified electrode were carried out using cyclic voltammetry (CV) and electrochemical impedance spectroscopy (EIS). These electrochemical studies were performed in a phosphate buffer containing 1.0 mM $Fe(CN)_6^{3-}/Fe(CN)_6^{4-}$ as the redox marker. Figure 2(a) shows the cyclic voltammograms recorded with bare SPCE, SPCE/MoS_2-QD, and SPCE/MoS_2-QD/PSA_{Ab}. The current density was greater than bare electrode when CV was recorded with MoS_2-QD modified electrode. However, after immobilization of PSA antibody, the current density decreased which is due to insulating characteristics of biomolecules. This also confirmed the immobilization of PSA antibody on the surface of MoS_2-QD modified SPCE. In Fig. S6, the I-V characteristics of bare SPCE and MoS_2-QD modified SPCE also depict the better conducting property of MoS_2-QDs than the bare SPCE. After immobilization of the PSA_{Ab}, both the anodic and cathodic peak current values decreased again, while the ΔEp increased (Fig. 2(a)). This decrease in the electrochemical response of the antibody-containing electrode is attributed to the non-conducting behavior of biomolecules.

In Fig. 2(b), the CV response of the SPCE/MoS_2-QD/PSA_{Ab} electrodes is plotted as a function of PSA concentration. The redox reaction of Fe^{3+}/Fe^{2+} ions is used as the signal for PSA detection. The peak current corresponding to the reduction of Fe^{3+} to Fe^{2+} decreased with an increase in PSA level due to the passivation of electrode surface that blocks the diffusion of the redox marker ions. This passivation is due to the presence of insulating layers formed by the PSA antibody-antigen complex. Figure 2(c) shows a linear relation between current density response and the logarithm of PSA concentration in the range from 0.1 pg·mL^{-1} to 10 ng·mL^{-1}. The linear regression equation was derived as y = (−0.3211)x + 7.835 (regression coefficient of 0.98). The sensitivity of the CV method calculated based on the slope analysis was 1.72 nAcm^{-2}/ng·mL^{-1}.

Figure 2(d) shows the impedance-based characterization results of the different types of modified electrodes, viz. SPCE/MoS_2-QD, SPCE/MoS_2-QD/PSA_{Ab} and SPCE/MoS_2-QD/$PSA_{Ab\text{-}PSA}$, in the form of Nyquist plots. These Nyquist plots consist of semicircles whose diameters change as the electrodes are sequentially modified. The semicircle pattern in the impedance spectra is representative of the electrical processes taking place in the material as well as in the vicinity of an electrode surface. The semicircle diameter corresponds to the electron/charge transfer resistance (R_{ct}), illustrating the electron transfer kinetics of the redox probe occurring at the electrode surface. The change in semicircle diameter is directly related to the change in R_{ct}. An increase in semicircle diameter correlates with increasing R_{ct}, and vice-versa. The characteristic shape of the Nyquist plots, as shown in Fig. 2(d), indicates that the electrode functions via a kinetics-controlled process. The inset in Fig. 2(d) shows the Randles

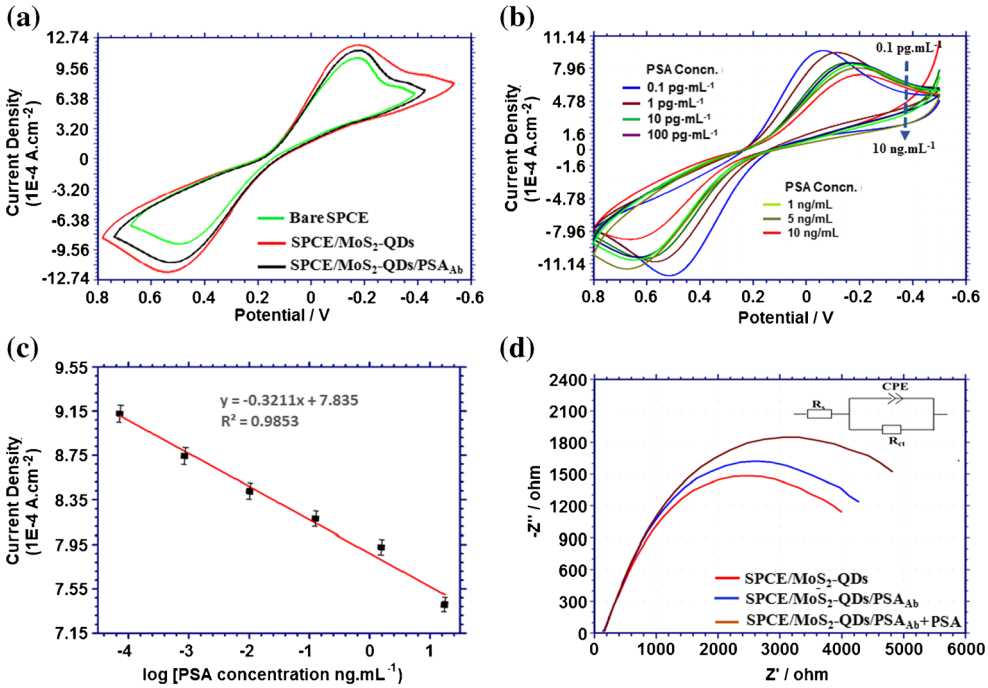

Fig. 2 Comparison of detection properties of MoS_2-QD electrodes under various combinations: (**a**) Cyclic voltammograms of modified electrodes in 1 mM $Fe(CN)_6^{3-}/Fe(CN)_6^{4-}$, (**b**) CV of SPCE/$MoS_2$-QD/$PSA_{Ab}$ electrodes as a function of PSA concentration, (**c**) Linearity graph (peak current values (Fig. 2b) plotted against log [PSA concentration, ng·mL^{-1}]), (**d**) Nyquist plot of modified electrodes in 1 mM $Fe(CN)_6^{3-}/Fe(CN)_6^{4-}$. Note that all the measurements with SPCE/MoS_2-QD, SPCE/MoS_2-QD/PSA_{Ab} and SPCE/MoS_2-QD/PSA_{Ab} + PSA electrodes were run in triplicate. The average variation in the estimated readings of R_{ct} was limited to ≤2.6%

equivalent circuit used to determine the values of R_{ct} through fitting of the impedance data. In this selected circuit, a constant phase element (non-ideal capacitance) is used in parallel with the R_{ct} component.

After the estimation of values, the MoS_2-QD modified electrode exhibits an R_{ct} value of 4.68 kΩ. This value further increased to 5.18 kΩ after the immobilization of anti-PSA antibodies. This suggests that the impedance characteristics are dominated by the electrostatic potential barrier for the negatively-charged redox marker. Upon incubating a 0.1 pg·mL^{-1} PSA (i.e., the antigen) with the SPCE/MoS_2-QD/PSA_{Ab} electrode, the R_{ct} increased to 5.85 kΩ due to the formation of affinity-based immune-complex and the resulting restriction of electron transfer. The EIS results are consistent with the results of cyclic voltammetry, which confirms the successful immobilization of the anti-PSA molecules onto the MoS_2-QD modified electrode surface.

Electrochemical assay of PSA using impedance spectrometry (EIS)

For the impedimetric immunoassay of PSA, seven SPCE/MoS_2-QD/PSA_{Ab} electrodes were incubated with different PSA concentrations (i.e, 0.01 pg·mL^{-1}, 0.1 pg·mL^{-1} 1.0 pg·mL^{-1}, 100 pg·mL^{-1}, 10 ng·mL^{-1}, 100 ng·mL^{-1}, 200 ng·mL^{-1}) for 15 min. The electrodes were then washed with phosphate buffer, and the EIS measurements were recorded in the presence of the standard redox marker. Figure 3(a) shows the Nyquist plots as a function of PSA concentration. As the concentration of PSA increased, a proportional rate of complex formation took place between the anti-PSA antibody and the antigen. The complex, having an insulating effect, created a barrier for the diffusion of Fe^{3+}/Fe^{2+} ions. This effect led to the increase in the value of impedance (described with R_{ct}). The change in R_{ct} was linear as a function of the logarithm of PSA concentration in the range of 0.01 pg·mL^{-1} - 200 ng·mL^{-1} [Fig. 3(b)]. The results of the impedance analysis were consistent with those obtained with CV; however, an extended range of analysis is observed with EIS. The analytical performance of the immunoassay was also compared with other similar procedures reported in the literature (Table S1). In the reported literature, various matrices have been used to attain different linear detection ranges, which can be attributed to the responsiveness of the transducer materials, as well as to the conjugation chemistry. The present method offers a comparatively wide range of analysis capability due to high surface area and well-suited semiconducting properties of the transducer material.

1×10^{-5} ng·mL^{-1} (or 0.01 pg·mL^{-1}) was found to be the practically attainable LOD of the method. Below this concentration value, the R_{ct} response of the electrodes was almost

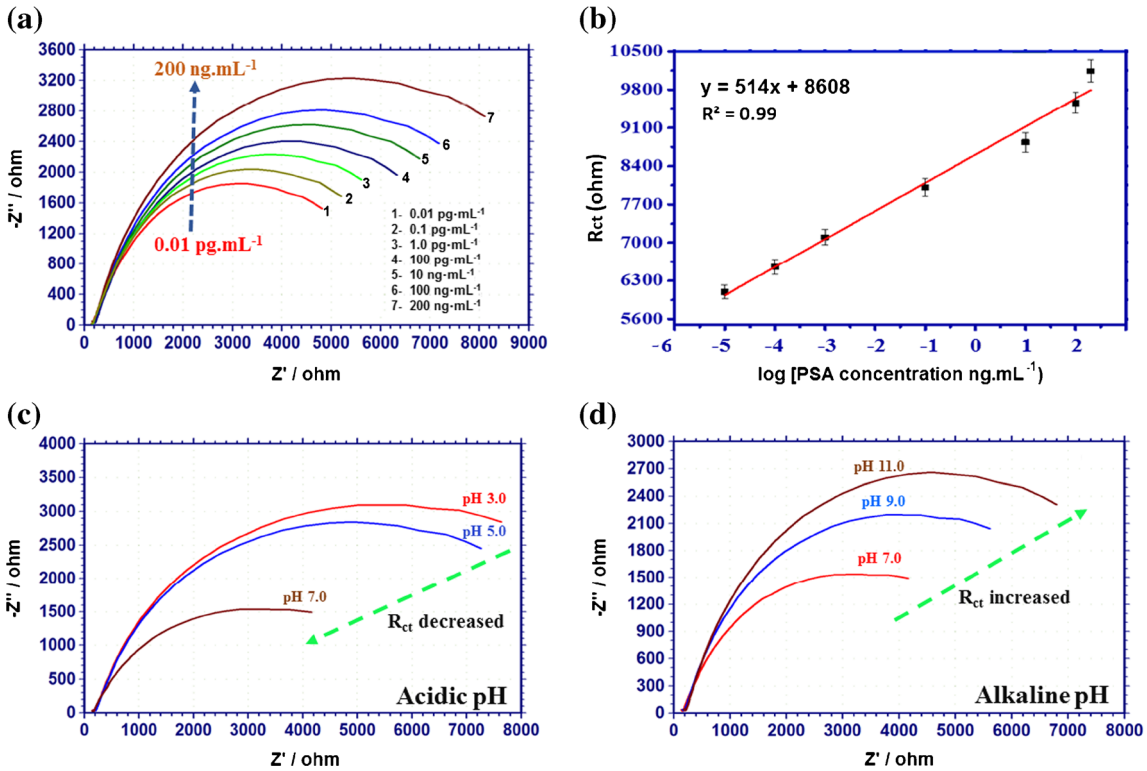

Fig. 3 Results of impedimetric analysis: (**a**) Impedimetric response of the SPCE/MoS_2-QD/PSA_{Ab} electrodes as a function of PSA concentration, (**b**) Linearity graph, (**c**) Impedimetric response of the SPCE/MoS_2–QD/PSA_{Ab} electrodes at acidic pH, (**d**) At alkaline pH. Note that all the measurements done with SPCE/MoS_2-QD/PSA_{Ab} + PSA electrodes were made as triplicate. The average variation in the estimated readings of R_{CT} was limited to ≤3.0%

identical (±5%) to that with the blank (0 PSA) concentration. We took a safe limit of R_{ct} variation as a minimum of 10% to distinguish the signals from the blank and the minimum quantifiable analyte concentration. The sensitivity of the EIS assay is estimated to be 2 mΩ/ng·mL^{-1}.

The pH of the redox probe may also play a vital role in the analytical response of the electrodes. A slight change of pH in the vicinity of biomolecules can hinder the access of the redox probes to the electrode surface. Therefore, we investigated the effect of pH on the response of the SPCE/MoS_2-QD/PSA_{Ab} electrodes. The R_{ct} value decreased from 9.5 kΩ to 5.67 kΩ as the pH value increased from 3.0 to 7.0 [Fig. 3(c)]. Beyond pH 7.0, the impedance value showed an increasing pattern [Fig. 3(d)]. The observed variation under alkaline pH conditions is due to the increase in the concentration of negatively-charged hydroxide ions (OH^- ions), which caused electrostatic repulsion between the negatively-charged PSA molecules and the electrode surface (containing OH^- ions). It should be noted that highly acidic or alkaline surroundings might cause damage to the immobilized protein structure. Therefore, the optimum pH of 7.0 is most suitable for practical applications.

The stability and reproducibility of the SPCE/MoS_2-QD/PSA_{Ab} electrodes were investigated by measuring EIS response of five different electrodes towards an analyte solution of 100 ng·mL^{-1} PSA. As shown in Fig. S7, all the five electrodes prepared in different modes displayed almost identical EIS responses, confirming the highly reproducible nature of the SPCE/MoS_2-QD/PSA_{Ab} electrodes. The immunoassay was also studied for its specificity by recording the response with respect to other proteins, namely human serum albumin (HSA), carcinoembryonic antigen, IgG and alpha-fetoprotein. An insignificant response was observed in the presence of even about 100-fold concentration of non-specific proteins, highlighting that the technique is highly specific for PSA [Fig. S8(a)]. The feasibility of the immunoassay for clinical applications was studied by measuring PSA concentrations in spiked serum samples. The human serum samples were spiked with known concentrations of the target antigens, and R_{ct} values were measured [Fig. S8(b), Table S2]. The values of R_{ct} for both standard and spiked samples are very close to each other, with acceptable percentage recovery values of 100 ± 2. These results also suggest good reproducibility for the MoS_2-QD modified bioelectrodes. The overall performance of the reported immunoassay thus demonstrates its potential in applications in clinical research and diagnosis.

Conclusions

The present research work was carried out to explore the use of MoS_2 QDs as a new material of choice for the fabrication of an electrochemical immunoassay system. Being a zero dimensional material, MoS_2-QDs have attractive electronic properties due to quantum confinement and edge effects. The combination of both large edge-to-volume ratios and high in-plane electron transport makes them potentially more attractive candidate than other nanostructured forms of MoS_2 with a larger band gap, better electrocatalytic activity, and enhanced breakage of intra-plane S–Mo–S bonds. As such they are capable of producing more edge atoms than the monolayer 2D sheets. A lack of coordination of the surface atoms also increases the density of unsaturated electron. Consequently, a high surface activity of MoS_2 QDs results in an improved electrocatalytic characteristics while the bioconjugation of proteins is facilitated by enhanced hydrophobicity. Thus, MoS_2 QDs are successfully synthesized and evaluated for potential as an immunoassay template. The QDs are used for modification of an SPCE surface to support the physical adsorption of antibodies. Compared to other matrices reported in the literature, the presence of MoS_2-QDs offers designing of an immunoassay with wide detection range capability. The SPCE/MoS_2-QD/PSA_{Ab} immunoassay also shows good selectivity and practical applicability with the spiked serum samples. The MoS_2 QD based bionanotemplate can be an attractive candidate for point-of-care diagnostic applications.

As a limitation of the herein proposed assay procedure, a fine control on the synthesis conditions is desirable to achieve uniformly distributed MoS_2 QDs. This is important because of the size dependent charge transfer properties of QDs. The design of the bioelectrodes has been kept simple by opting hydrophobic attachment of the antibodies over the MoS_2 surface; however, this makes the electrode to work as a single-shot assay. More investigations may be carried out in future to improve the robustness and recyclability of the MoS_2-QD based immunoassays.

Acknowledgements The authors are thankful to the Director of CSIR-CSIO, Chandigarh, India. M.K is thankful to the Council of Scientific and Industrial Research (CSIR), New Delhi, India, for granting the Senior Research Fellowship (SRF). We acknowledge the research funding from CSIR India via research grant no. MLP-023. KHK acknowledges the support made in part by grants from the National Research Foundation of Korea (NRF) funded by the Ministry of Education, Science and Technology (MEST) (No. 2016R1E1A1A01940995) and the support of "Cooperative Research Program for Agriculture Science and Technology Development (Project No. PJ012521032017)" Rural Development Administration, Republic of Korea.

Compliance with ethical standards The author(s) declare that they have no competing interests.

References

1. Peng Q, De S (2013) Outstanding mechanical properties of monolayer MoS 2 and its application in elastic energy storage. Phys Chem Chem Phys 15(44):19427–19437
2. El Beqqali O, Zorkani I, Rogemond F, Chermette H, Chaabane RB, Gamoudi M, Guillaud G (1997) Electrical properties of

molybdenum disulfide MoS2. Experimental study and density functional calculation results. Synth Met 90(3):165–172
3. Gaur AP, Sahoo S, Ahmadi M, Dash SP, Guinel MJ-F, Katiyar RS (2014) Surface energy engineering for tunable wettability through controlled synthesis of MoS2. Nano Lett 14(8):4314–4321
4. Stephenson T, Li Z, Olsen B, Mitlin D (2014) Lithium ion battery applications of molybdenum disulfide (MoS 2) nanocomposites. Energy Environ Sci 7(1):209–231
5. Kukkar M, Sharma A, Kumar P, Kim K-H, Deep A (2016) Application of MoS 2 modified screen-printed electrodes for highly sensitive detection of bovine serum albumin. Anal Chim Acta 939: 101–107
6. Wang T, Zhu H, Zhuo J, Zhu Z, Papakonstantinou P, Lubarsky G, Lin J, Li M (2013) Biosensor based on ultrasmall MoS2 nanoparticles for electrochemical detection of H2O2 released by cells at the nanomolar level. Anal Chem 85(21):10289–10295
7. Zhu C, Zeng Z, Li H, Li F, Fan C, Zhang H (2013) Single-layer MoS2-based nanoprobes for homogeneous detection of biomolecules. J Am Chem Soc 135(16):5998–6001
8. Govindasamy M, Chen S-M, Mani V, Akilarasan M, Kogularasu S, Subramani B (2017) Nanocomposites composed of layered molybdenum disulfide and graphene for highly sensitive amperometric determination of methyl parathion. Microchim Acta 184(3):725–733
9. Xing L, Ma Z (2016) A glassy carbon electrode modified with a nanocomposite consisting of MoS2 and reduced graphene oxide for electrochemical simultaneous determination of ascorbic acid, dopamine, and uric acid. Microchim Acta 183(1):257–263
10. Aghagoli MJ, Shemirani F (2017) Hybrid nanosheets composed of molybdenum disulfide and reduced graphene oxide for enhanced solid phase extraction of Pb (II) and Ni (II). Microchim Acta 184(1):237–244
11. Gao Z, Lin Y, He Y, Tang D (2017) Enzyme-free amperometric glucose sensor using a glassy carbon electrode modified with poly (vinyl butyral) incorporating a hybrid nanostructure composed of molybdenum disulfide and copper sulfide. Microchim Acta 184(3): 807–814
12. Lin Y, Chen X, Lin Y, Zhou Q, Tang D (2015) Non-enzymatic sensing of hydrogen peroxide using a glassy carbon electrode modified with a nanocomposite made from carbon nanotubes and molybdenum disulfide. Microchim Acta 182(9–10):1803–1809
13. He B (2017) Differential pulse voltammetric assay for the carcinoembryonic antigen using a glassy carbon electrode modified with layered molybdenum selenide, graphene, and gold nanoparticles. Microchim Acta 184(1):229–235
14. Li Y, Lin H, Peng H, Qi R, Luo C (2016) A glassy carbon electrode modified with MoS2 nanosheets and poly (3, 4-ethylenedioxythiophene) for simultaneous electrochemical detection of ascorbic acid, dopamine and uric acid. Microchim Acta 183(9):2517–2523
15. Yang T, Chen H, Yang R, Jiang Y, Li W, Jiao K (2015) A glassy carbon electrode modified with a nanocomposite consisting of molybdenum disulfide intercalated into self-doped polyaniline for the detection of bisphenol a. Microchim Acta 182(15–16):2623–2628
16. Mani V, Govindasamy M, Chen S-M, Karthik R, Huang S-T (2016) Determination of dopamine using a glassy carbon electrode modified with a graphene and carbon nanotube hybrid decorated with molybdenum disulfide flowers. Microchim Acta 183(7):2267–2275
17. Lin T, Zhong L, Chen H, Li Z, Song Z, Guo L, Fu F (2017) A sensitive colorimetric assay for cholesterol based on the peroxidase-like activity of MoS2 nanosheets. Microchim Acta 184(4):1233–1237
18. Zhou X, Wan L-J, Guo Y-G (2013) Synthesis of MoS 2 nanosheet–graphene nanosheet hybrid materials for stable lithium storage. Chem Commun 49(18):1838–1840
19. Yin W, Yan L, Yu J, Tian G, Zhou L, Zheng X, Zhang X, Yong Y, Li J, Gu Z (2014) High-throughput synthesis of single-layer MoS2 nanosheets as a near-infrared photothermal-triggered drug delivery for effective cancer therapy. ACS Nano 8(7):6922–6933
20. Wang L, Wang Y, Wong JI, Palacios T, Kong J, Yang HY (2014) Functionalized MoS2 Nanosheet-based field-effect biosensor for label-free sensitive detection of cancer marker proteins in solution. Small 10(6):1101–1105
21. Jemal A, Siegel R, Ward E, Murray T, Xu J, Smigal C, Thun MJ (2006) Cancer statistics, 2006. CA Cancer J Clin 56(2):106–130. https://doi.org/10.3322/canjclin.56.2.106
22. Rao AR, Motiwala HG, Karim O (2008) The discovery of prostate-specific antigen. BJU Int 101(1):5–10
23. Kukkar M, Tuteja SK, Sharma AL, Kumar V, Paul AK, Kim K-H, Sabherwal P, Deep A (2016) A new electrolytic synthesis method for few-layered MoS2 Nanosheets and their robust biointerfacing with reduced antibodies. ACS Appl Mater Interfaces 8(26):16555–16563
24. Kaur J, Arya VP, Kaur G, Raychaudhuri T, Lata P (2012) Evaluation of ultrasonic treatment for the size reduction of HNS and HMX in comparison to solvent-Antisolvent crystallization. Propellants, Explosives, Pyrotechnics 37(6):662–669
25. Gu W, Yan Y, Zhang C, Ding C, Xian Y (2016) One-step synthesis of water-soluble MoS2 quantum dots via a hydrothermal method as a fluorescent probe for hyaluronidase detection. ACS Appl Mater Interfaces 8(18):11272–11279
26. Benson J, Li M, Wang S, Wang P, Papakonstantinou P (2015) Electrocatalytic hydrogen evolution reaction on edges of a few layer molybdenum disulfide nanodots. ACS Appl Mater Interfaces 7(25):14113–14122
27. Lee J, Dak P, Lee Y, Park H, Choi W, Alam MA, Kim S (2014) Two-dimensional layered MoS2 biosensors enable highly sensitive detection of biomolecules. Sci Rep 4:7352. https://10.1038/srep07352
28. Su S, Zou M, Zhao H, Yuan C, Xu Y, Zhang C, Wang L, Fan C, Wang L (2015) Shape-controlled gold nanoparticles supported on MoS 2 nanosheets: synergistic effect of thionine and MoS 2 and their application for electrochemical label-free immunosensing. Nanoscale 7(45):19129–19135
29. Lee C, Yan H, Brus LE, Heinz TF, Hone J, Ryu S (2010) Anomalous lattice vibrations of single-and few-layer MoS2. ACS Nano 4(5):2695–2700
30. Chen C, Qiao H, Lin S, Luk CM, Liu Y, Xu Z, Song J, Xue Y, Li D, Yuan J (2015) Highly responsive MoS2 photodetectors enhanced by graphene quantum dots. Sci Rep 5:11830
31. Gopalakrishnan D, Damien D, Shaijumon MM (2014) MoS2 Quantum dot-interspersed exfoliated MoS2 nanosheets. ACS Nano 8(5):5297–5303
32. Chikan V, Kelley D (2002) Size-dependent spectroscopy of MoS2 nanoclusters. J Phys Chem B 106(15):3794–3804
33. Kukkar M, Tuteja SK, Sharma AL, Kumar V, Paul AK, Kim K-H, Sabherwal P, Deep A (2016) A new electrolytic synthesis method for few-layered MoS2 Nanosheets and their robust biointerfacing with reduced antibodies. ACS Appl Mater Interfaces 8(26):16555–16563. https://doi.org/10.1021/acsami.6b03079
34. Wilcoxon J, Newcomer P, Samara G (1997) Synthesis and optical properties of MoS 2 and isomorphous nanoclusters in the quantum confinement regime. J Appl Phys 81(12):7934–7944